Diffusion of atomic hydrogen in an atmospheric-pressure free-burning arc discharge

S. C. Snyder,[1] A. B. Murphy,[2] D. L. Hofeldt,[3] and L. D. Reynolds[1]
[1]*Idaho National Engineering Laboratory, P.O. Box 1625, Idaho Falls, Idaho 83415*
[2]*Commonwealth Scientific and Industrial Research Organisation, Division of Applied Physics, P.O. Box 218, Lindfield, New South Wales 2070, Australia*
[3]*Department of Mechanical Engineering, 111 Church Street Southeast, University of Minnesota, Minneapolis, Minnesota 55455*
(Received 26 April 1995)

Relative radial concentration profiles of atomic hydrogen in an atmospheric-pressure argon-hydrogen free-burning 200-A arc discharge were measured using laser-induced fluorescence by two-photon excitation of the ground state of atomic hydrogen. Radial profiles are presented for three axial locations. A comparison between the measured profiles and profiles calculated using a diffusion model that considers demixing processes is made. The measured profiles decrease less rapidly with increasing radius than the calculated profiles, suggesting, in agreement with calculations, that the diffusion rate of atomic hydrogen is greater than the recombination rate. Consequently, local chemical equilibrium is not maintained at larger radii in the arc.

PACS number(s): 52.25.Fi, 51.20.+d, 51.10.+y, 52.70.−m

I. INTRODUCTION

Thermal plasmas are often composed of a mixture of an inert gas and a molecular gas such as hydrogen, oxygen, or nitrogen. When molecular species dissociate, not only is plasma chemistry influenced, but the enthalpy of the plasma is increased and heat transfer to particles in the plasma or to substrates is enhanced. Diffusion due to concentration, temperature, and pressure gradients, together with the influence of external forces, can actually lead to a separation of the reactive atomic species from the inert gas [1]. This can greatly alter the physical properties of the plasma.

The diffusion of gases in plasmas has been examined theoretically by several authors using the Chapman-Enskog method [2]. In order to model diffusion coefficients, most authors define an equilibrium composition of the plasma. However, an equilibrium description of the plasma as given by the Saha equation is not appropriate for two-temperature plasmas. There is strong experimental evidence that atmospheric-pressure plasmas are not in local thermodynamic equilibrium (LTE); in fact, the electron temperature is often significantly greater than the heavy-particle temperature [3]. Deviation from LTE could imply that the plasma also deviates from local chemical equilibrium (LCE).

A complete understanding of diffusion in mixed-gas plasmas requires experimentally determined species-concentration profiles in order to validate diffusion models. Emission spectroscopy is a suitable diagnostic technique for determining species-concentration profiles if the plasma is in LTE and optically thin. Laser-induced fluorescence (LIF) on the other hand does not depend on LTE to determine species-concentration profiles. Additionally, LIF can detect atoms in regions of the plasma where the temperature is too low to excite appreciable emission. Finally, LIF is not a line-of-sight technique and does not, in contrast to emission spectroscopy, require an Abel inversion of the data. Hence, a high degree of spatial resolution is possible. A potentially serious drawback is that LIF spectra can be quite complex if collisional redistribution of the population of the laser-excited state is significant. Furthermore, photoionization of species in the plasma by the incident laser beam is a possible problem, especially in multiphoton-excitation schemes [4].

Hydrogen is one of the most common reactive gases added to plasmas. Because of its low mass and small atomic radius, atomic hydrogen is expected to have a high diffusion rate. Also, the net effect of collisions (demixing due to collision-frictional forces) is to concentrate the lighter species in the high temperature region of the plasma. This has been observed in argon-hydrogen arcs [5,6]. Verification of diffusion models might therefore best be accomplished by comparing predicted ground-state atomic hydrogen density profiles with measured profiles.

Single-photon laser excitation of the ground state of atomic hydrogen is not possible with lasers presently available because the transitions are at vacuum-ultraviolet wavelengths. However, multiphoton excitation of ground-state atomic hydrogen is possible and has been demonstrated in flames and plasmas [4,7]. We report in this paper relative concentration profiles of atomic hydrogen in an argon-hydrogen atmospheric-pressure free-burning arc discharge determined by two-photon laser excitation of the ground state. The measured profiles are compared with profiles calculated using a local chemical equilibrium model that includes the effects of demixing [8], a diffusive process that leads to separation of the reactive and inert gases. Use of the combined diffusion coefficient formulation [2] greatly simplifies the treatment of demixing, and allows the different physical processes contributing to the demixing to be identified.

Discrepancies between the measured and calculated hydrogen densities in the fringe region of the arc are examined in terms of deviations from LCE due to the rapid diffusion of atomic hydrogen.

II. THEORY OF ARC COMPOSITION

The simplest description of the composition of an arc containing more than one chemical element is that the relative concentration of each of the chemical elements is constant everywhere in the arc, and that the concentrations of the species containing these elements are those calculated assuming LCE. LCE implies that the composition at any given position in the arc is that for which the Gibbs free energy is minimized for the local temperature and the local chemical element concentrations, or equivalently, that the composition satisfies the Guldberg-Waage and Saha equations.

Diffusion can lead to significant variations from this description. The relevant diffusion-driven processes can be conveniently divided into two types, according to whether they lead to departures from LCE. We will use the term demixing [8,9] to describe those diffusion processes that lead to spatial variations in the relative concentrations of the chemical elements within the arc, while not causing departures from LCE. Those processes that lead to departures from LCE occur when the diffusion rate of a given species is large compared to the rate of ionization, dissociation, recombination, or other chemical reactions involving that species. Such processes generally require steep temperature gradients. Unlike demixing, departures from LCE due to rapid diffusion can occur in single-element as well as multielement arcs.

Diffusion is described by the equation for the number flux of the species i relative to the mass-average velocity in a gas mixture containing q species [10,11]:

$$\mathbf{g}_i \equiv n_i \mathbf{v}_i = \frac{n^2}{\rho} \sum_{j=1}^{q} m_j D_{ij} \nabla x_j - \frac{D_i^T}{m_i} \nabla \ln T \ , \tag{1}$$

where $\mathbf{v}_i$ is the diffusion velocity of species i relative to the mass average velocity; D_{ij} and D_i^T are, respectively, ordinary and thermal diffusion coefficients; T is the temperature; n and ρ are, respectively, the number density and mass density; and x_j, n_j, and m_j are, respectively, the mole fraction, number density, and mass of the jth species. Diffusion due to gradients in the total pressure and due to external forces is neglected in Eq. (1). In an ionized gas, D_{ij} and D_i^T are calculated so as to include ambipolar diffusion effects [2,11].

Equation (1) can be used to describe both demixing processes and deviations from LCE due to diffusion. However, because of the large number of species q that occur in arcs in mixtures of gases, and since there are $q(q-1)/2$ linearly independent ordinary diffusion coefficients and the $q-1$ linearly independent thermal diffusion coefficients, such a description becomes very complicated.

Murphy [2] has shown that in many cases, the ordinary and thermal diffusion coefficients may be replaced by a total of three combined diffusion coefficients, which describe the diffusion of two gases relative to one another. The conditions under which this can be done are that the two gases are homonuclear and do not react with each other, and that the concentrations of the individual species depend only on the temperature and the relative concentrations of the two gases. The latter condition is satisfied when LCE exists.

The combined diffusion coefficient approach is thus appropriate to treatment of demixing, but is not applicable when diffusion rates are sufficiently large relative to reaction rates that deviations from LCE occur. We will briefly review the combined diffusion coefficient approach, and apply it to calculate the effect of demixing on the hydrogen concentration in an arc, in Sec. II A. The method of calculation of relative rates of diffusion and recombination of atomic hydrogen, which may be used to explain some of the discrepancies between the measured and calculated profiles, will be outlined in Sec. II B.

A. Combined diffusion coefficients and demixing

The combined diffusion coefficients are defined in a mixture of two gases, denoted A and B, by an expression for the number flux of gas A, of the same form as Eq. (1) for a two-species gas:

$$\overline{\mathbf{g}_A} = \frac{n^2}{\rho} \overline{m_B} \overline{D_{AB}^x} \nabla \overline{x_B} - \frac{\overline{D_{AB}^{T1}} + \overline{D_A^T}}{\overline{m_A}} \nabla \ln T \ , \tag{2}$$

where $\overline{m_B}$ is the average mass of the heavy species of gas B. The bar notation is used to denote properties that are averaged or summed over all species in a gas from those of a single species. Murphy [2] derived expressions for the combined diffusion coefficients, $\overline{D_{AB}^x}$, $\overline{D_{AB}^{T1}}$, and $\overline{D_A^T}$ by combining with Eqs. (1) and (2) the definition of $\overline{\mathbf{g}_A}$:

$$\overline{\mathbf{g}_A} = \sum_i s_i \mathbf{g}_i \ , \tag{3}$$

where the s_i's are stoichiometric coefficients and the sum is over all species belonging to gas A.

If the mass-average velocity is small compared to the diffusion velocities, we can neglect convection, and the equilibrium mole fraction gradients of the two gases may be calculated by setting $\overline{\mathbf{g}}_A = \mathbf{0}$ in Eq. (2), giving

$$\nabla \overline{x_B} = -\nabla \overline{x_A} = \frac{\rho}{n^2} \frac{(\overline{D_{AB}^{T1}} + \overline{D_A^T}) \nabla \ln T}{\overline{m_A}\,\overline{m_B}\,\overline{D_{AB}^x}} \ . \tag{4}$$

A comparison of calculated diffusion rates and the convective velocities predicted by numerical models of free-burning arcs [12] indicates that it is reasonable to neglect convection except within about 0.5 mm of the arc axis, where convective (or mass-average) velocities reach 300 $\mathrm{m\,s^{-1}}$.

Murphy [9] has shown that the three diffusion coefficients $\overline{D_{AB}^x}$, $\overline{D_{AB}^{T1}}$ and $\overline{D_A^T}$ describe demixing due to different phenomena; respectively, demixing due to mole fraction gradients, due to frictional or collisional forces, and due to thermal diffusion. The classification of the demixing phenomena was introduced by Frie and Maecker [8,13]. Demixing due to mole fraction (or partial pres-

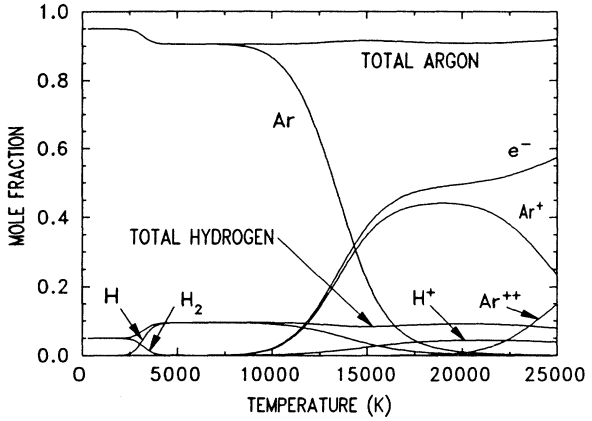

FIG. 1. Equilibrium mole fractions in a mixture of 95% argon and 5% hydrogen by mole fraction at a pressure of 101.3 kPa, neglecting demixing effects. Species with mole fractions less than 0.001 over the full temperature range are not shown. The total mole fractions of argon and hydrogen include electrons derived from the ionization of the respective gases.

sure) gradients occurs to minimize the gradients $\nabla \overline{x_A} = -\nabla \overline{x_B}$. Demixing due to frictional forces occurs due to the unbalanced collisional, or frictional, forces acting on the different species, and often leads to significant deviations from $\nabla \overline{x_A} = 0$. Thermal diffusion, described by the last term in Eq. (1), can also lead to significant demixing.

Figure 1 shows the equilibrium mole fractions of the main species in a mixture of hydrogen and argon as a function of temperature in the absence of demixing. Calculations were performed using a code originally developed by Svehla and McBridge [14], modified to allow treatment of charged species [15]. The Debye-Hückel correction is taken into account, but the effect of ionization potential lowering is neglected. Calculations for the equilibrium composition of a pure hydrogen plasma show excellent agreement for temperatures up to 25 000 K with the data of Patch [16], who considered both the Debye-Hückel correction and the effects of ionization potential lowering.

It can be seen in Fig. 1 that the total hydrogen mole fraction $\overline{x_H}$ increases as the temperature increases through the dissociation temperature of molecular hydrogen. In the presence of a spatial temperature gradient, we would expect demixing due to the resulting mole fraction gradient to lead to a net flux of hydrogen to the low temperature region, in order to minimize $\nabla \overline{x_H}$. Figures 2(a) and 2(b) show the combined diffusion coefficients $\overline{D^x_{Ar,H}}$, $\overline{D^{T1}_{Ar,H}}$ and $\overline{D^T_{Ar}}$ as a function of temperature in a mixture of hydrogen and argon. The method of calculation of the ordinary diffusion coefficients D_{ij} and thermal diffusion coefficients D_i^T, in calculating the combined diffusion coefficients, is described in the Appendix. We note that the ratio $(\overline{D^T_{Ar,H}} + \overline{D^T_{Ar}})/\overline{D^x_{Ar,H}}$ is positive at all temperatures below 22 500 K; hence Eq. (4) predicts a net flux of argon to lower temperature regions and hence a

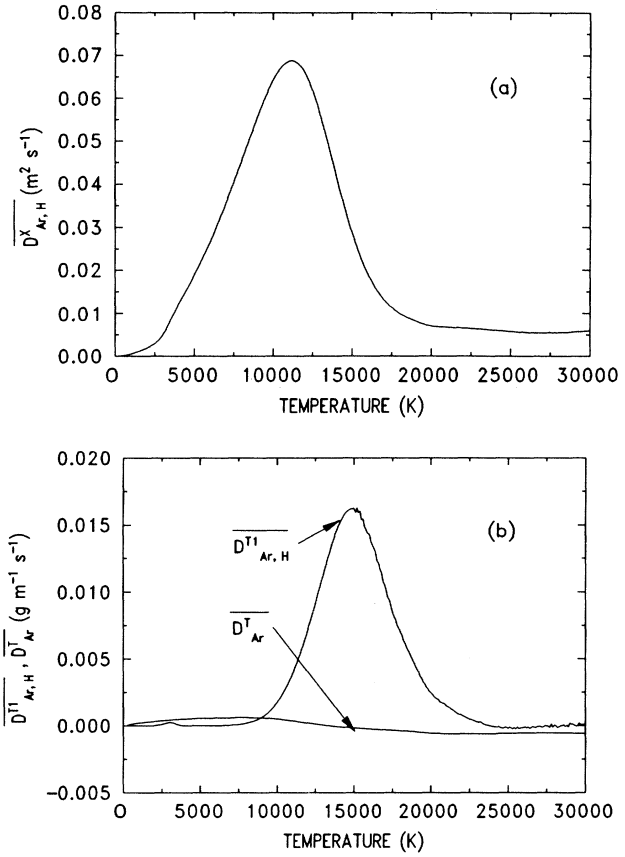

FIG. 2. Combined diffusion coefficients for a mixture of 95% argon and 5% hydrogen by mole fraction as a function of temperature. (a) is $\overline{D^x_{Ar,H}}$ as a function of temperature and (b) is $\overline{D^{T1}_{Ar,H}}$ and $\overline{D^T_{Ar}}$ as a function of temperature.

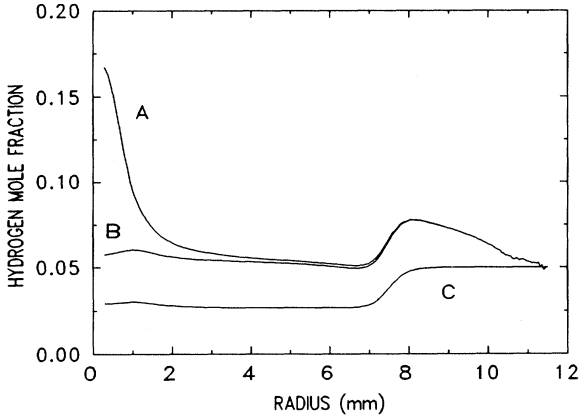

FIG. 3. Total hydrogen mole fraction in a mixture of 95% argon and 5% hydrogen by mole fraction, calculated using the radial temperature profile shown in Fig. 4 for 2.5 mm below the cathode in an argon arc. Curve *A* is all three demixing processes taken into account. Curve *B* is only demixing due to partial pressure gradients and thermal diffusion taken into account. Curve *C* is only demixing due to partial pressure gradients taken into account.

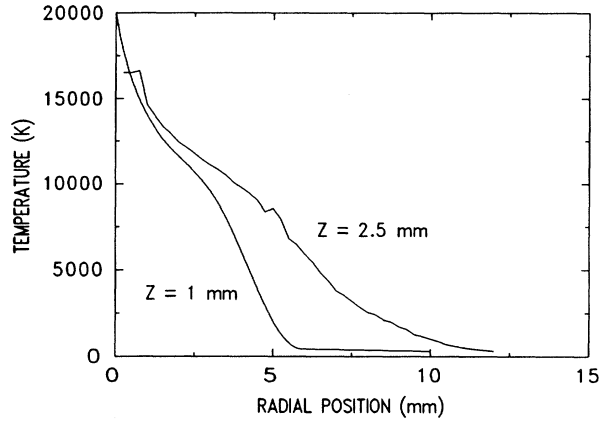

FIG. 4. Radial temperature profiles of a 200-A argon arc with a 5-mm gap determined from frequency-integrated laser light scattering. Data are presented at axial positions of 1 mm and 2.5 mm below the cathode.

flux of hydrogen to the higher temperature regions. This effect is due to both frictional forces and thermal diffusion, the former being dominant for 10 000 K $< T <$ 22 500 K since $D^{T1}_{\mathrm{Ar,H}} > D^{T}_{\mathrm{Ar}}$ for this temperature range, and the latter for $T <$ 10 000 K since D^{T}_{Ar} is larger at these lower temperatures.

Figure 3 shows the total hydrogen mole fraction in a mixture of argon and hydrogen, calculated taking the different demixing phenomena into account. The calculations use the gas temperature profile shown in Fig. 4. These temperatures were determined in an all-argon arc using a frequency-integrated Thomson-Rayleigh laser light scattering technique described elsewhere [17]. The values shown in Fig. 3 were calculated by numerically integrating Eq. (4) in one dimension, radially from the edge of the arc to the center. The composition at the edge is assumed to be the input or nondemixed composition. The effect of demixing due to partial pressure gradients only is calculated by setting $D^{T1}_{AB} = D^{T1}_{A} = 0$ in Eq. (4). The effect of thermal diffusion is added by keeping $D^{T1}_{AB} = 0$ and giving D^{T}_{A} its calculated value.

Figure 3 shows, as predicted in the foregoing discussion, that an increase in hydrogen mole fraction is observed at low temperatures (below 4000 K in this case) and high temperatures (above 13 000 K in this case). These increases are seen to be due to demixing due to partial pressure gradients and thermal diffusion at low temperatures and demixing due to frictional forces at high temperatures.

B. Departures from LCE due to diffusion

The diffusion velocity of a given species, for example, atomic hydrogen, in a gas mixture containing q species is given by Eq. (1). The q ordinary diffusion coefficients and the thermal diffusion coefficient required are calculated as described in the Appendix.

Recombination of atomic hydrogen to form molecular hydrogen occurs through the three-body reaction $H+H+M \rightarrow H_2+M$, where M represents any third body. The rate of recombination of atomic hydrogen to form molecular hydrogen is given by

$$d[\mathrm{H}]/dt = 2k[\mathrm{H}]^2[M] = -2k[\mathrm{H}]^2[M] , \quad (5)$$

where [H], for example, is the molecular concentration of atomic hydrogen. The rate coefficient k is 7.0×10^{17} $\mathrm{cm^6\,mol^{-2}\,s^{-1}}\,T(\mathrm{K})^{-1}$, where T(K) is the temperature in kelvin, for M = Ar [18]. From Eq. (5), the average lifetime of a hydrogen atom before recombination is

$$\tau \equiv -[\mathrm{H}]/(d[\mathrm{H}]/dt) = \frac{1}{2k[\mathrm{H}][M]} . \quad (6)$$

III. EXPERIMENT

A. Multiphoton processes

There are several techniques available for multiphoton excitation of the ground state of atomic hydrogen. These techniques, discussed in detail elsewhere [4], are based on either single-wavelength two-photon, two-wavelength (2+1)-photon, or single-wavelength three-photon excitation of the ground state to the $n=3$ or 4 level. The fluorescence transition monitored is either the $n=3$ to $n=2$ (H_α) transition at 656.3 nm or the $n=4$ to $n=2$ (H_β) transition at 486.1 nm. The experimental setup for two-photon excitation is considerably simpler than for (2+1)-photon excitation. Hence, the two 205-nm excitation scheme, depicted in Fig. 5, is preferred and was used in this work.

The dependence of the two-photon fluorescence signal on the intensity of the incident laser beam is quadratic if the fluorescence is far from saturation and photoionization of the laser-excited state is not significant [4]. Because of the difficulty in quantifying photoionization processes in plasmas, it is preferable to experimentally verify that the signal satisfies this quadratic dependence. Because the fluorescence signal is not saturated in this case, care must be taken to assure that the laser intensity remains constant during the course of a measurement.

The ground-state population density of atomic hydrogen is proportional to the product of the fluorescence signal and a quantum efficiency factor, or

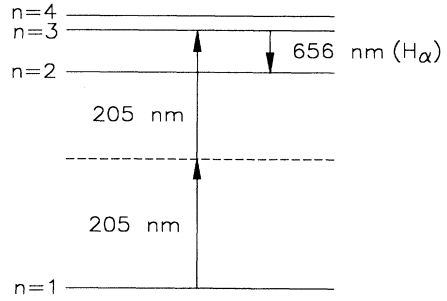

FIG. 5. Partial energy-level diagram of atomic hydrogen showing the two-photon excitation scheme.

$$[\mathrm{H}] \propto \frac{A_{31}+A_{32}+R}{A_{32}} I_F \ , \tag{7}$$

where A_{32} and A_{31} are the spontaneous decay rates from the $n=3$ to $n=2$ levels and the $n=3$ to $n=1$ levels, respectively, and R is the collisional quenching rate. For this work, argon is the predominant collision partner with hydrogen, and we have

$$R = k_{\mathrm{Ar}}[\mathrm{Ar}] \ . \tag{8}$$

In Eq. (8), the quenching rate coefficient $k_{\mathrm{Ar}} = \langle \sigma v \rangle$ where σ is the quenching cross section and v is the relative velocity of the excited hydrogen atom and the argon atom.

B. Experimental setup

The 205-nm laser wavelength was generated by frequency-tripling the 615-nm output of a neodymium-doped yttrium aluminum garnet (Nd:YAG) pumped pulsed-dye laser operated with sulfarhodamine dye. The output of the Nd:YAG laser was 532 nm with a pulse rate of 30 Hz and pulse width of 10 ns. Frequency-tripling was accomplished using a potassium dihydrogen phosphate (KD*P) crystal to frequency-double the fundamental dye laser output to 308 nm. This was followed by mixing the dye laser fundamental and doubled frequencies in a β-barium borate (BBO) crystal to generate the 205-nm wavelength. The efficiency of 205-nm wavelength generation was increased by using a telescope to reduce the laser beam waist by a factor of about 3 in the BBO crystal. A half-wave plate was used to rotate the plane of polarization of the 615-nm wavelength beam 90° to make it parallel to the plane of polarization of the 315-nm beam to maximize mixing efficiency in the BBO crystal. This half-wave plate was also used to adjust the energy of the 205-nm beam by detuning the polarization alignment. Approximately 0.9 mJ pulse^{-1} of laser energy was obtainable at 205 nm using a pump energy of 300 mJ pulse^{-1} at 532 nm. After the BBO crystal, a Pellin-Broca prism separated the laser beam into its three wavelength components. A 200-mm focal length lens focused the 205-nm beam into the plasma. The fluorescence signal was collected by 300-mm achromatic lenses and focused at a magnification of 1 to 1 onto the entrance slit of a 1-m focal-length monochromator with an 1800-groove mm^{-1} grating. The entrance and exit slits were 150 μm wide resulting in a monochromator bandwidth of about 0.08 nm. A horizontal slit approximately 300 μm wide was placed over the entrance slit so that only the waist of the focused laser beam was imaged on the entrance slit. This greatly improved the signal-to noise ratio by reducing background signal from the plasma continuum radiation. A Hamamatsu R928 photomultiplier tube (PMT) was used to detect the fluorescence signal. The PMT signal was integrated using a gated dual-channel boxcar averager averaging over 30 shots of the laser. The first channel of the boxcar averager integrated the signal over a 50-ns gate while the second channel, triggered about 50 ns later, integrated the plasma background over a 50-ns gate. The integrated background level was then subtracted from the integrated signal level, and the result digitized and stored on a computer. A schematic of the experimental setup is given in Fig. 6.

All data were taken on a free-burning transferred argon-hydrogen arc at atmospheric pressure operating over a water-cooled copper anode. The nominal hydrogen concentrations of the gas mixtures studied were 5% and 1% by mole fraction in argon. A gas-chromatography analysis of these gas mixtures indicated that the actual compositions used were 94.6% argon–6.4% hydrogen and 99% argon–1% hydrogen, respectively. The diameter of the 2%-thoriated tungsten cathode was 2.4 mm. A conical tip with an included angle of 60° was ground on the end of the cathode. The cathode-to-anode gap was 5 mm. The arc current was 200 A and the total gas flow was about 8 l min^{-1}.

IV. RESULTS AND DISCUSSION

While absolute concentration measurements of the ground state of atomic hydrogen are possible with careful

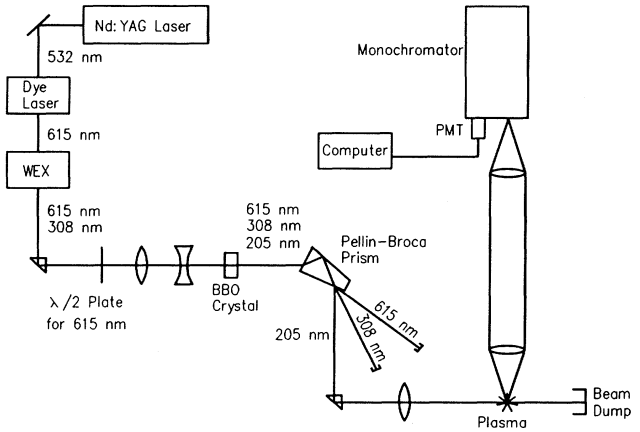

FIG. 6. Experimental schematic. WEX is a wavelength extender which is a frequency-doubling crystal of KD*P, and $\lambda/2$ waveplate is a half-wave plate.

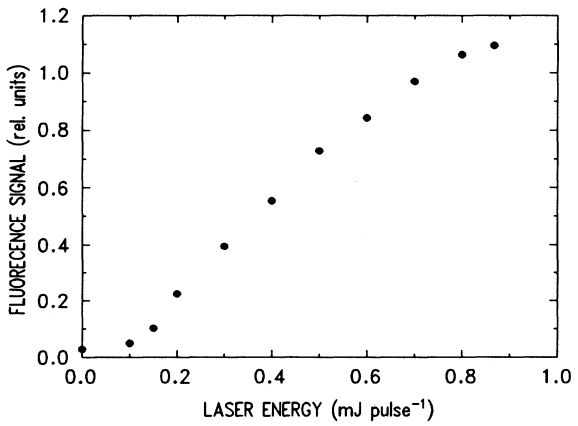

FIG. 7. Two-photon laser-induced fluorescence signal as a function of laser energy.

calibration of the two-photon LIF signal, for the purposes of this work, only relative concentration measurements were made. Figure 7 shows the relative two-photon LIF signal strength at 656 nm of atomic hydrogen in the arc as a function of laser energy. The data were taken at 2.5 mm below the cathode at a radial position of 7 mm. At low laser energies, the relationship between the signal and laser energy is quadratic. At higher laser energies, the signal definitely begins to saturate. Based on this curve, all data were taken at a laser energy of 0.4 mJ pulse^{-1}. It was felt that this laser energy resulted in a good signal-to-noise ratio while minimizing the effects of photoionization on the signal.

We now compare the measured ground-state atomic hydrogen concentrations with calculated distributions. It should first be noted that the discussion of arc composition in Sec. II A referred to all energy levels of atomic hydrogen, whereas in fact only the ground-state atoms are detected in the measurements. However, we calculate that under LTE, the maximum excited atom density (i.e., the maximum difference between the total atomic hydrogen and the ground-state atomic hydrogen densities) is about 5×10^{20} m^{-3}, which is only 0.3% of the maximum atomic hydrogen density. The calculation is based on the fact that the internal partition function of atomic hydrogen under LTE conditions is almost exactly equal to 2 over the full temperature range for which its density is not negligible [19,20].

Figures 8(a) and 8(b) and Figs. 9(a) and 9(b) compare the measured and calculated radial profiles of the atomic hydrogen density at 1 mm and 2.5 mm below the cathode, respectively, for 5% and 1% hydrogen by mole fraction in argon. Profiles calculated both neglecting and including the effects of demixing are given for positions 1 mm and 2.5 mm below the cathode. The calculations were based on the temperature profiles measured using laser scattering for a 200-A argon arc, which are shown

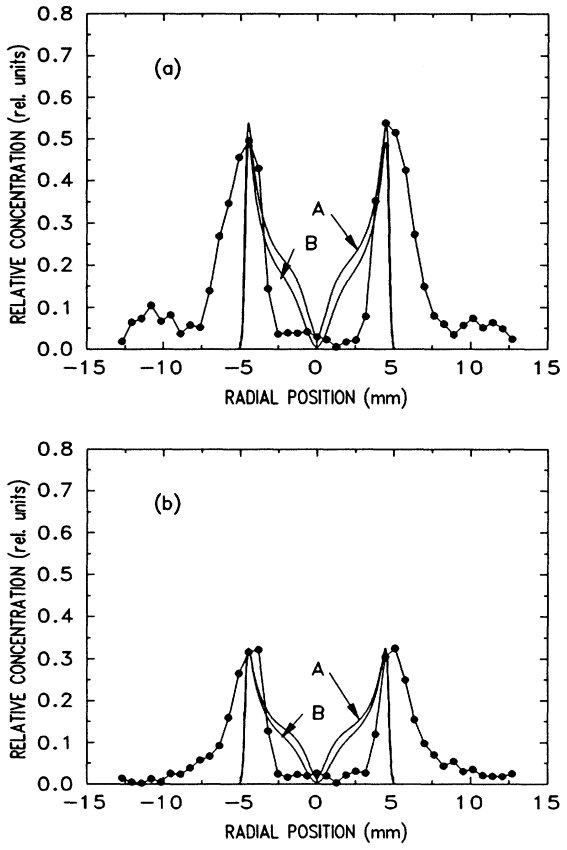

FIG. 8. Relative ground-state atomic hydrogen density as a function of radial position, calculated including (curve A) and excluding (curve B) the effects of demixing, compared with the measured values at the axial positions of 1 mm below the cathode. Results are given for both 5% and 1% hydrogen by mole fraction in argon in (a) and (b), respectively. The calculated curves are normalized with respect to the peak of the measured values. The calculations used the temperature profiles measured by laser scattering at the corresponding axial positions, shown in Fig. 4.

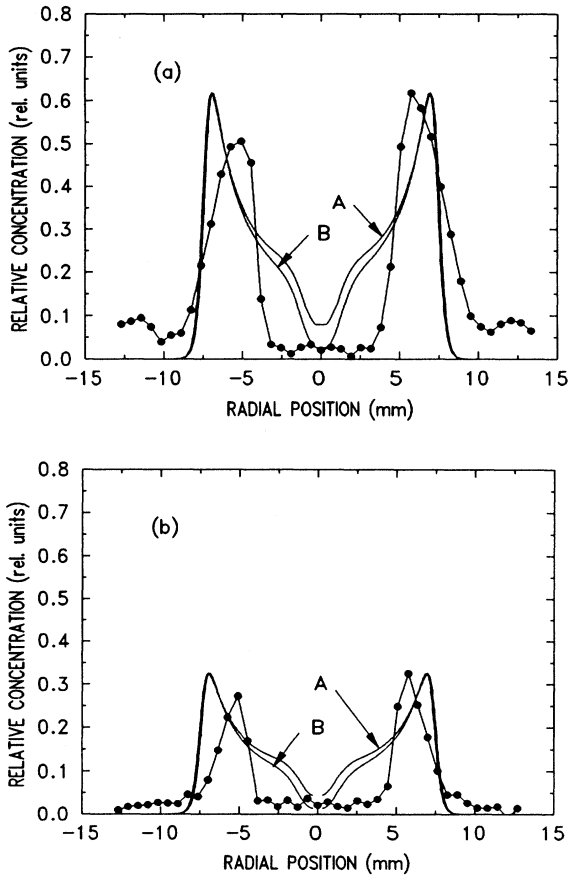

FIG. 9. Relative ground-state atomic hydrogen density as a function of radial position, calculated including (curve A), and excluding (curve B) the effects of demixing, compared with the measured values at the axial positions of 2.5 mm below the cathode. Results are given for both 5% and 1% hydrogen by mole fraction in argon (a) and (b), respectively. The calculated curves are normalized with respect to the peak of the measured values. The calculations used the temperature profiles measured by laser scattering at the corresponding axial positions, shown in Fig. 4.

in Fig. 4. The measured and calculated positions of the peak in the atomic hydrogen density differ slightly at both positions. The discrepancies probably arise from two effects. First, there are likely to be small differences between the axial position used for measurements of hydrogen density profiles and for the temperature measurements, because the measurements were performed on a different apparatus, making it difficult to ensure that the thermal expansion of the cathode was compensated for equally in both measurements. Second, the measured temperature distribution of a pure argon arc was used in calculating the atomic hydrogen distribution. This is expected to lead to errors. The addition of hydrogen to an argon arc will increase its thermal conductivity, and is expected to narrow the arc column, thus decreasing the temperature in the fringe regions of the arc. Taking this second effect into account in the calculation of the atomic hydrogen density profiles would decrease the radius of the peaks, improving the agreement between the experimental and calculated results. Simulations using the code described by Lowke, Kovitya, and Schmidt [12] show that this effect is larger further from the cathode. Figure 10 is the measured relative atomic hydrogen radial profile 4 mm below the cathode. Gas temperature data were not possible to obtain this close to the anode because of excessive stray laser light, so calculated profiles are not presented.

Three further discrepancies are apparent between the measured and calculated profiles. First, the measured hydrogen density decreases radially towards the arc center to almost zero within 2.5 mm of the peak. This agrees qualitatively with similar measurements made on a free-burning arc discharge at a pressure of 0.5 atm [21]. However, the calculated density is still approximately 50% of its maximum value at this position. Second, the measured profile decreases much less rapidly than the calculated profile from the peak towards the arc edge. Third, the measured profiles demonstrate secondary peaks at radii greater than 10 mm; these are not reflected in the calculated profiles.

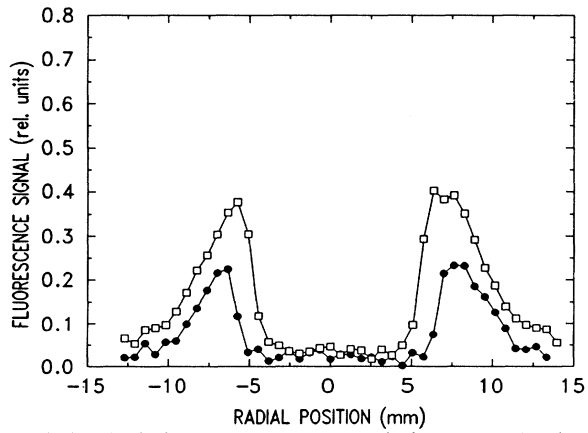

FIG. 10. Relative ground-state atomic hydrogen density as a function of radial position measured 4 mm below the cathode. The open squares and solid curves are for 5% and 1% hydrogen by mole fraction in argon, respectively. Calculated profiles are not available for this case.

The first discrepancy can probably be explained in terms of Stark broadening of the H_α signal that is detected. The electron density in atmospheric-pressure free-burning arc discharges is on the order of 1.5×10^{23} m^{-3} in the arc column [22]. At these electron densities, the Stark-broadened linewidth of the H_α transition is about 1 nm [21,23], which is much broader than the bandwidth of the monochromator. One cannot be certain if the lack of a fluorescence signal in the center of the arc is because there is not a detectable amount of atomic H present or because only a small portion of the Stark-broadening signal overlaps with the bandwidth of the monochromator. It is therefore meaningless to compare the measured profile with the predicted profile in this region. The electron density decreases rapidly with increasing radial position, and hence also the degree of Stark broadening of the H_α transition. It was verified that the linewidth of the peak fluorescence signal was less than 0.05 nm at radial positions greater than 5 mm.

The second discrepancy between the measured and calculated atomic hydrogen density profiles may be attributed to the large diffusion rate of atomic hydrogen relative to the rate of recombination to form molecular hydrogen. Figure 11(a) shows as a function of radius the diffusion distance d_H of atomic hydrogen before recombination, defined as the absolute value of the product of the diffusion velocity v_H and the lifetime τ before recombination of atomic hydrogen. Plots of v_H and τ as a function of radius are presented in Figs. 11(b) and 11(c), respectively. Note that d_H is zero at the cusps in Fig. 11(a), since v_H passes through zero at these radii. Atomic hydrogen diffuses inwards at radii between the cusps, and outwards elsewhere. The mole fraction gradients used in Eq. (1) to calculate the diffusion velocity are derived from the temperature profile shown in Fig. 4 assuming an LCE composition.

The diffusion velocity is very large, and directed radially outward, at radii greater than that of the peak in the atomic hydrogen density n_H. In this region, the dominant diffusion mechanism is ordinary diffusion, with the terms in $D_{H,Ar}\nabla x_{Ar}$ and $D_{H,H_2}\nabla x_{H_2}$ being the largest in Eq. (1). In the temperature range 5000 to 8000 K, corresponding to radii less than that of the peak in n_H, the mole fraction gradients of all species are small [see Fig. (1)] and thermal diffusion dominates. In this region, v_H is directed toward the arc axis. At still smaller radii, atomic hydrogen again diffuses outward, with the ordinary diffusion terms $D_{H,Ar^+}\nabla x_{Ar^+}$ and $D_{H,H^+}\nabla x_{H,H^+}$ dominating. Note that in this region, ionization reactions will decrease the diffusion distance of atomic hydrogen below that given by d_H.

It can be seen that in the fringe regions the diffusion distance is very large compared to the dimensions of the arc, which indicates that an LCE composition will not be maintained in these regions. Since the direction of the diffusion is toward larger radii, an anomalously large atomic hydrogen concentration is expected at the edge of the arc.

Figure 11(a) indicates that d_H increases rapidly to very large values at large radii. Note, however, that d_H is cal-

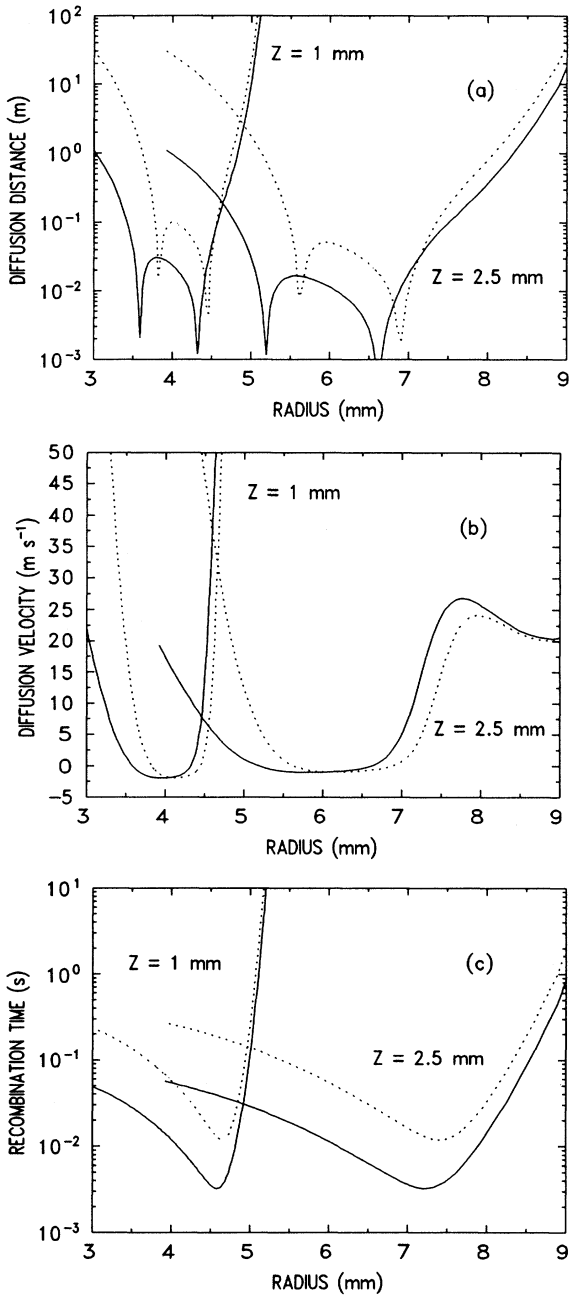

FIG. 11. Calculated radial dependence of (a) the absolute value of the diffusion distance, (b) the radial diffusion velocity, and (c) the recombination time of atomic hydrogen in mixtures of 5% (solid line) and 1% (dotted line) hydrogen in argon by mole fraction at axial positions of 1 mm and 2.5 mm below the cathode. The calculations used the temperature profiles shown in Fig. 4. The radial diffusion velocity is defined to be positive when directed toward the edge of the arc.

culated assuming an LCE composition. The diffusion time τ is approximately inversely related to the atomic hydrogen density, and v_H is similarly inversely related through n_H and also through the gradient terms ∇x_{H_2} and ∇x_{Ar}, which decrease when ∇x_H increases. Hence, an increase in the density of atomic hydrogen above the LCE value will strongly decrease the diffusion distance d_H. Thus, recombination will dominate over diffusion at sufficiently large radii.

It is further worth noting that the rapid diffusion of atomic hydrogen cannot move the position of the peak in atomic hydrogen density to a larger radius than that calculated assuming the existence of LCE. This is because the position of the peak in n_H is determined by the equilibrium chemistry, occurring at that temperature at which recombination of atomic hydrogen is in equilibrium with the dissociation of molecular hydrogen. At larger radii, no matter how large the diffusion flux of atomic hydrogen, the dominance of recombination reactions will cause a decrease in n_H. In fact, a large diffusion flux of atomic hydrogen can, counterintuitively, lead to the peak in n_H being shifted to a smaller radius, since an increase in n_H increases the temperature at which recombination and dissociation reactions are in equilibrium. This effect is, however, relatively small, since the equilibrium temperature only increases from 3940 to 4390 K when the mole fraction of atomic hydrogen is increased from 0.05 to 0.50.

The final discrepancy, the occurrence of secondary peaks in the measured atomic hydrogen density at large radii, is more difficult to explain. The temperature at the position of the peaks is less than 1000 K according to Fig. 4; this is well below the dissociation temperature of molecular hydrogen. One possibility that the peaks were due to photodissociation of molecular hydrogen due to the laser beam was considered, but the peaks disappeared when the arc was extinguished. The fact that the peaks occur at smaller radii at axial positions closer to the cathode suggests that they may be due to a nonideality in the flux coming from the nozzle. Another possibility, recirculation of hot gas upward away from the anode, seems unlikely because significant upward velocities are not predicted by numerical models of free-burning arcs such as that described by Lowke, Kovitya, and Schmidt [12].

In the above discussion, collisional effects on the measured fluorescence signals were not considered. Only the H_α transition was observed indicating collisional redistribution of the population of the laser-excited state to higher states was not significant. However, the effect of collisional quenching to lower states is significant, and its effect on the measured relative concentration profiles can be estimated as follows. The quenching rate coefficient k_{Ar} for atomic hydrogen in the $n=3$ state colliding with argon has been measured at room temperature to be 4.6×10^{-16} m^{3}s^{-1} [24]. The collisional quenching cross section is assumed to be constant over the temperature range of interest in this experiment (300 to 9000 K). Consequently, the collisional quenching rate given by Eq. (8) is proportional to $T^{-1/2}$. Using Eq. (7) and the data of Figs. 1 and 4, the measured fluorescence signals can be corrected to include the effects of collisional quenching. The corrected fluorescence signals are compared to the measured signals for the 95% argon–5% hydrogen gas mixture at 1 mm and 2.5 mm below the cathode in Figs. 12(a) and 12(b), respectively. Since argon is the primary

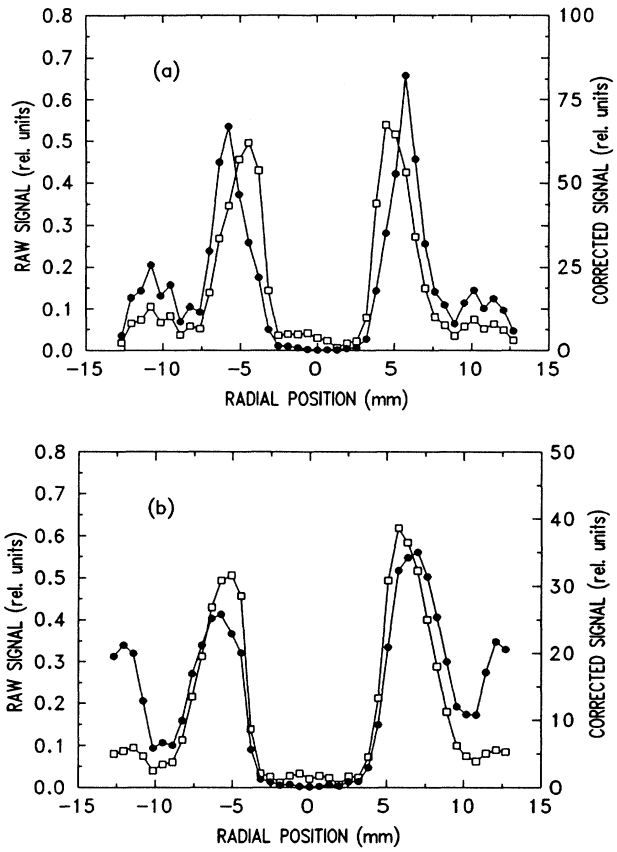

FIG. 12. A comparison of the raw relative fluorescence signals as a function of radial position with signals corrected for collisional quenching. The open squares are the raw signal values and the solid circles are the corrected signal values. The data were taken at (a) 1 mm below the cathode and (b) 2.5 mm below the cathode in a 95% argon–5% hydrogen gas mixture.

collision partner with hydrogen, the effect of collisional quenching on the measured fluorescence signals for the 99% argon–1% hydrogen gas mixture data should be similar to the 95% argon–5% hydrogen gas mixture case. Accounting for collisional quenching significantly increases the magnitude of the relative fluorescence signal. However, for the purposes of this work, the shape of the relative hydrogen concentration profile is of greater interest. The primary peaks of the hydrogen concentration occur at somewhat larger radial positions in the corrected profiles, strengthening our original observation that the diffusion rate of atomic hydrogen is greater than the recombination rate. The most interesting feature of the corrected profiles is a notable enhancement of the secondary peaks observed in the fringe region. The cause of these peaks becomes even more intriguing, and certainly warrants further investigation.

V. CONCLUSIONS

Diffusion processes in an atmospheric-pressure argon-hydrogen arc discharge were studied using two-photon laser-induced fluorescence to determine relative radial concentration profiles of the ground state of atomic hydrogen. Measured profiles were then compared to calculated profiles. The diffusion processes occurring in the arc were divided into two types, according to whether they led to departures from LCE. The term demixing was used to describe those processes which led to spatial variations in the relative concentrations of the chemical elements, but not to deviations from LCE. Using the combined diffusion coefficient formulation, it was calculated that demixing can lead to large increases in hydrogen concentration in the arc column. Unfortunately, it was not possible to test this prediction using the experimental data, since Stark broadening of the H_α emission in the arc column meant that the atomic hydrogen density could not be measured with any accuracy in this region.

The measured profiles of atomic hydrogen density were found to decrease less rapidly with increasing radius at temperatures below the recombination temperature of atomic hydrogen than predicted by calculations based on LCE. The discrepancy was explained by demonstrating that the diffusion rate of atomic hydrogen is larger than its recombination rate in this region. It may be concluded that LCE is not maintained in the low temperature region of the arc due to the rapid diffusion of atomic hydrogen.

ACKNOWLEDGMENTS

This work was supported by the U.S. Department of Energy, Office of Energy Research, Office of Basic Energy Sciences, under DOE Operations Office, Idaho, Contract No. DE-AC07-94ID13223.

APPENDIX: CALCULATION OF DIFFUSION COEFFICIENTS

The diffusion coefficients D_{ij} and D_i^T defined by Eq. (1) were calculated using the Chapman-Enskog method [10,11,25]. They were obtained by solving sets of coupled linear equations, the terms of which are functions of the number densities and masses of the species and of collision integrals $\Omega_{ij}^{(l,s)}$ of each pair of species i and j.

The collision integrals are given by

$$\Omega_{ij}^{(l,s)}=\frac{4(l+1)}{\pi(s+1)![2l+1-(-1)^l]} \times\int_0^\infty e^{-\gamma^2}\gamma^{2s+3}Q_{ij}^{(l)}(g)\,d\gamma\ , \tag{A1}$$

where $\gamma^2=\mu g^2/2kT$, μ and g being, respectively, the reduced mass and the relative speed of species i and j, and where $Q_{ij}^{(l)}(g)$ are the gas-kinetic cross sections, given by

$$Q_{ij}^{(l)}(g)=2\pi\int_0^\infty(1-\cos^l\chi)b\,db\ . \tag{A2}$$

Here b is the impact parameter and χ is the deflection angle, which is a function of b, g, and the intermolecular potential $V(r)$, r being the separation of the interacting particles [10,26].

Diffusion coefficients were calculated to a second-order approximation, i.e., retaining two terms in the finite Sonine polynomial used in the Chapman-Enskog method. This required the calculation of the collision integrals

with $(l,s)=(1,1)$, (1,2), (1,3), and (2,2). Collisions between all important species, i.e., Ar, Ar^+, Ar^{2+}, Ar^{3+}, H_2, H_2^+, H, H^+, and H^-, were considered. The collision integrals were calculated either by numerical integration of experimental data for the momentum-transfer cross section $Q_{ij}^{(l)}(g)$ using Eq. (A1), or from published intermolecular potentials using Eqs. (A1) and (A2). Momentum-transfer cross sections were obtained from published tabulations or from charge-exchange cross section, Q_{ex}, data using the relation $Q^{(l)}(g)=2Q_{ex}$ [27]. Collision integrals were obtained from intermolecular potentials using the data of Monchick [28] for exponential repulsive potentials, Brokaw [29] for exponential attractive potentials, Kihara, Taylor, and Hirschfelder [30] for inverse power potentials, including polarization potentials, and Mason, Munn, and Smith [31] for the screened Coulomb potential; numerical integration using the method of Barker, Fock, and Smith [32] was used for all other potentials.

The intermolecular potentials and momentum-transfer cross-section data for the Ar-Ar, Ar^+-Ar, and *e*-Ar interactions were those used by Murphy and Arundell [33]. For the H_2-H_2, H-H, Ar-H, Ar^+-H, H^+-H, and *e*-H interactions the data selected by Aubreton and Fauchais [34] were employed. The H_2-H interaction was described using the potential tabulated by Boothroyd *et al.* [35], and the H_2-Ar interaction by the Morse–spline–van der Waals potential given by Dunker and Gordon [36].

The $l=1$ collision integrals for the H^+-H_2, H_2^+-Ar, and Ar^+-H_2 interactions were calculated from the momentum-transfer and charge-exchange cross sections given by Phelps [37,38]; the corresponding integrals for the H_2^+-H_2 interaction were calculated from the charge-exchange cross section given by Vance and Bailey [39]. The $l=s=2$ collision integrals for all these interactions, and all collision integrals for the H_2^+-H and H^--H interactions, were calculated using the polarization potential (an inverse power potential given, for example, by Murphy and Arundell [33]). An exponential repulsive potential fitted to the data of Stärk and Meyer [40] and the modified Morse potential of Kuntz and Roach [41] were used for the H^--H_2 and the H^+-Ar interactions, respectively.

The momentum-transfer cross-section data selected by Itikawa [42], supplemented at low energies by the data of Crompton *et al.* [43], were used for the *e*-H_2 interaction. Collision integrals for interactions between charged species were calculated using the screened Coulomb potential [31], the screening distance being set equal to the Debye radius. The calculation of collision integrals in ionized gases is discussed in greater detail in many publications [33,34,44].

[1] J. R. Fincke, C. H. Chang, W. D. Swank, and D. C. Haggard, Int. J. Heat Mass Transfer **37**, 1673 (1994).

[2] A. B. Murphy, Phys. Rev. E **48**, 3594 (1993).

[3] S. C. Snyder, L. D. Reynolds, J. R. Fincke, G. D. Lassahn, J. D. Grandy, and T. E. Repetti, Phys. Rev. E **50**, 519 (1994).

[4] J. E. M. Goldsmith and N. M. Laurendeau, Opt. Lett. **15**, 576 (1990).

[5] W. Kasparek, K. Hirsch, and E. Holzauer, Plasma Phys. **22**, 555 (1980).

[6] J. B. Shumaker, Jr. and C. H. Popenoe, Phys. Rev. Lett. **21**, 1046 (1968).

[7] D. Wagner, V. Schultz-von der Gathen, H. F. Döbele, and A. T. Young, *ESCAMPIG 92: Eleventh European Sectional Conference on the Atomic and Molecular Physics of Ionized Gases, St. Petersburg, Russia, 1992,* edited by L. Tsendin (European Physical Society, Geneva, 1992), p. 273.

[8] W. Frie and H. Maecker, Z. Phys. **162**, 69 (1961).

[9] A. B. Murphy, Phys. Rev. Lett. **73**, 1797 (1994).

[10] J. O. Hirschfelder, C. F. Curtiss, and R. B. Bird, *Molecular Theory of Gases and Liquids,* 2nd ed. (Wiley, New York, 1964).

[11] R. S. Devoto, Phys. Fluids **9**, 1230 (1966).

[12] J. J. Lowke, P. Kovitya, and H. P. Schmidt, J. Phys. D **25**, 1600 (1992).

[13] W. Frie, Z. Phys. **172**, 99 (1963).

[14] R. A. Svehla and B. J. McBride, NASA Technical Note No. NASA TN D-7056, 1973 (unpublished).

[15] P. Kovitya, CSIRO Division of Applied Physics Technical Memo. No. 3, 1982 (unpublished).

[16] R. W. Patch, NASA Special Publication NASA SP-3069, 1971 (unpublished).

[17] A. B. Murphy, J. Phys. D **27**, 1492 (1994).

[18] N. Cohen and K. R. Westberg, J. Phys. Chem. Ref. Data **12**, 531 (1983).

[19] H.-W. Drawin and P. Fellenbok, *Data for Plasmas in LTE* (Gauthiers Villiers, Paris, 1965).

[20] K. Chen and T. L. Eddy, J. Non-Equilib. Thermodyn. **19**, 1 (1993).

[21] V. Schulz-von der Gathen, Ph.D. dissertation, University of Essen, 1990.

[22] S. C. Snyder, G. D. Lassahn, and L. D. Reynolds, Phys. Rev. E **48**, 4124 (1993).

[23] H. R. Griem, *Plasma Spectroscopy* (McGraw-Hill, New York, 1964).

[24] J. Bittner, K. Kohse-Höinghaus, U. Meier, and Th. Just, Chem. Phys. Lett. **143**, 571 (1988).

[25] S. Chapman and T. G. Cowling, *The Mathematical Theory of Non-Uniform Gases,* 3rd ed. (Cambridge University Press, Cambridge, England, 1970).

[26] J. H. Ferziger and H. G. Kaper, *Mathematical Theory of Transport Processes in Gases* (North-Holland, Amsterdam, 1972).

[27] A. Dalgarno, Philos. Trans. R. Soc. London **250**, 426 (1958).

[28] L. Monchick, Phys. Fluids **2**, 695 (1959).

[29] R. S. Brokaw, Phys. Fluids **4**, 944 (1961).

[30] T. Kihara, M. H. Taylor, and J. O. Hirschfelder, Phys. Fluids **3**, 715 (1960).

[31] E. A. Mason, R. J. Munn, and F. J. Smith, Phys. Fluids **10**, 1827 (1967).

[32] J. A. Barker, W. Fock, and F. Smith, Phys. Fluids **7**, 897 (1964).

[33] A. B. Murphy and C. J. Arundell, Plasma Chem. Plasma

Process. **14**, 451 (1994).
[34] J. Aubreton and P. Fauchais, Rev. Phys. Appl. **18**, 51 (1983).
[35] A. I. Boothroyd, W. J. Keogh, P. G. Martin, and M. R. Peterson, J. Chem. Phys. **95**, 4343 (1991).
[36] A. M. Dunker and R. G. Gordon, J. Chem. Phys. **68**, 700 (1978).
[37] A. V. Phelps, J. Phys. Chem. Ref. Data **19**, 653 (1990).
[38] A. V. Phelps, J. Phys. Chem. Ref. Data **21**, 883 (1992).
[39] D. W. Vance and T. L. Bailey, J. Chem. Phys. **44**, 486 (1966).
[40] J. Stärk and W. Meyer, Chem. Phys. **176**, 83 (1993).
[41] P. J. Kuntz and A. C. Roach, J. Chem. Soc. Faraday Trans. II **68**, 259 (1972).
[42] Y. Itikawa, At. Data Nucl. Data Tables **21**, 69 (1974).
[43] R. W. Compton, D. K. Gibson, and A. I. McIntosh, Aust. J. Phys. **22**, 715 (1969).
[44] M. Capitelli, J. Phys. (Paris) Colloq. **38**, C3-227 (1977).